J Mater Sci (2009) 44:2218–2225
DOI 10.1007/s10853-008-3025-z

FESTSCHRIFT IN HONOUR OF PROF T R ANANTHARAMAN ON THE OCCASION OF HIS 80TH BIRTHDAY

TEM and 3D atom probe characterization of DMS4 cast nickel-base superalloy

K. Muraleedharan · R. Balamuralikrishnan · N. Das

Received: 10 June 2008 / Accepted: 30 September 2008 / Published online: 5 November 2008

Abstract Cast nickel-base superalloys possess the required mechanical properties (creep resistance and stress rupture life) at elevated temperatures that make them suitable for turbine blades in aero-engines. The origin of these properties lies in the presence of a simple two phase γ–γ' microstructure (with cuboidal γ' particles dispersed in a γ matrix), in spite of the presence of several alloying elements. The cuboidal nature of the γ' particles arises from an optimal misfit between the two phases, which is a function of the composition of γ and γ' phases. In addition, several microstructural issues arising out of the partitioning of the alloying elements influences directly the deformation mechanisms in the γ and γ', and therefore the mechanical properties of the alloy. In this article, we discuss how some of these microstructural issues have been investigated in DMS4, a cast single crystal superalloy, experimentally using TEM and 3DAP techniques.

Abbreviations

TEM	Transmission electron microscopy
3DAP	3-dimensional atom probe
CBED	Convergent beam electron diffraction
HOLZ	Higher order Laue zone

Introduction

The objective of this article is to highlight the utility of combined transmission electron microscope (TEM) and 3-dimensional atom probe (3DAP) characterization of nanoscale features in DMS4, a cast single crystal nickel-base superalloy, in order to understand the microstructural effects on the mechanical properties. The knowledge thus gained can be used to tune the processing parameters to result in microstructures with desired properties. Whereas this article concentrates on a specific material, namely DMS4, the approach has a much wider applicability to nickel-base superalloys in general.

Nickel-base superalloys are the materials of choice for elevated temperature structural applications such as aeroengine components. Cast single crystal nickel-base superalloys, designed for use in aeroturbine applications, perform at high homologous temperatures (>0.7 T_M) and have to meet a demanding set of mechanical properties that include creep resistance and stress rupture life. Over decades of superalloys research [1], it has been established that a microstructure consisting of a high volume fraction (usually between 60% and 80%) of ~500 nm cuboidal particles of γ' (crystal structure: $L1_2$), dispersed uniformly in a disordered fcc matrix (γ) meets these challenges. While most nickel base superalloys are fundamentally based on Ni_3Al, the alloy design and development of these materials, dictated by the desire of having ever-increasing service temperatures, has resulted in contemporary superalloys having several different alloying elements (such as Co, Cr, Ta, W, and Re for instance) that influence the processing, (micro)structure, and the properties of the material.

DMS4 is a third generation single crystal nickel-base superalloy developed by the Defence Metallurgical Research Laboratory [2, 3] for turbine blade applications. Single crystal turbine blades are produced using the investment casting process involving directional solidification using a helical crystal selector [2]. The desired final

K. Muraleedharan (✉) · R. Balamuralikrishnan · N. Das
Defence Metallurgical Research Laboratory, Kanchanbagh PO, Hyderabad 500058, India
e-mail: muraleek@hotmail.com

microstructure, consisting predominantly of γ and γ' is achieved by subjecting the as-cast components to complex multi-step solutionizing and multi-step aging treatments [2, 3]. In the fully heat-treated condition, DMS4 offers more than 80 °C metal temperature advantage over the first generation single crystal superalloy CMSX2 and about 8 °C advantage over modern third generation alloys such as CMSX10. The nominal composition of DMS4 is given in Table 1. The alloy has a density of 9.08 g/cc and a total refractory content of 21.4 wt% including 6.5 wt% Re to provide improved creep resistance. Mo and Ti have been completely eliminated in order to ensure adequate phase stability.

The microstructure and composition in a turbine blade (Fig. 1a) typically vary over several length scales. During the solidification process, which proceeds by the formation and growth of dendrites (Fig. 1b), the alloying elements partition between the dendritic and interdendritic regions, at characteristic length scales of about 100 μm (Fig. 1c). The dendrites can further thought to be composed of a dendritic core (DC) and secondary dendrite arms (SDAs). Concurrently, within the dendrites, there is also alloying element partitioning between γ and γ' phases, on a much smaller scale of approximately 1 μm or less (Fig. 1d). This partitioning is present in the interdendritic regions (IDR) as well, but in addition to γ and γ', carbides are also present, and when the solidification is complete, the scale of the microstructure in these regions tends to be coarser than in the dendrites, of the order of a few micrometers. It should be noted that the size and shape of γ' in the as-cast condition vary widely in the different regions and that the subsequent processes of solutionizing and aging are essential to achieve the final desired microstructure.

The partitioning of alloying elements between the dendritic and interdendritic regions is usually determined using electron probe microanalysis. Figure 1e shows the composition of DC, SDA, and IDR in an as-cast DMS4 sample. The composition values represent the averages of at least 15 different measurements taken from each of the three

Table 1 Nominal composition of DMS4 alloy

	Cr	Co	W	Re	Ta	Hf	Nb	Al	Ni
wt%	2.4	4	5.5	6.5	9	0.1	0.3	5.2	Balance
at%	2.94	4.33	1.91	2.23	3.17	0.04	0.21	12.29	Balance

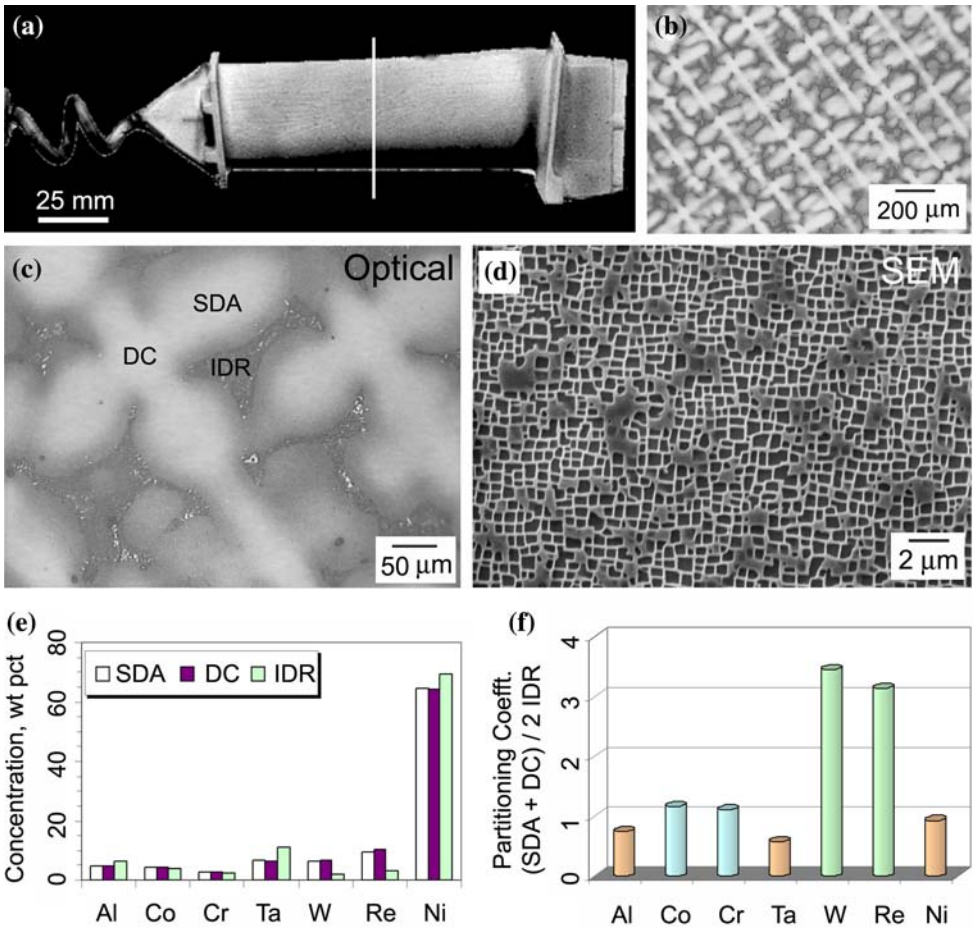

Fig. 1 The multi-scale nature of the microstructure in nickel-base superalloys, extending from the macroscopic scale down to ~500 nm, the typical size of the cuboidal γ': **a** Single crystal turbine blade; **b**, **c** optical micrographs at different magnifications of a transverse section indicated in (**a**) in the as-cast condition; **d** SEM micrograph of a fully heat-treated DMS4 sample showing cuboidal γ' particles in γ matrix; **e** partitioning of alloying elements between the dendrite core (DC), secondary dendritic arm (SDA) and inter-dendritic regions (IDR); and **f** ratio of partitioning between dendritic and interdendritic regions

areas. It can be seen that DC and SDA have quite similar composition, which differs substantially from the IDR composition. Figure 1f shows the ratio of the dendritic (taken as the average of DC and SDA) composition to the IDR composition. It can be seen that while tungsten and rhenium segregate strongly to the solidifying dendrites (ratio > 1), Ta, Al, and Ni (although weakly) are concentrated in IDR. Cobalt and chromium have a partitioning ratio close to unity suggesting a fairly uniform distribution in both dendrites and interdendritic regions. It must be noted that the difference in the compositions between the regions is largely diminished, but not eliminated, by the complex multi-step homogenizing (solutionizing) treatment.

As mentioned earlier, after the completion of the complex solutionizing and aging heat treatments, the sub-micron scale microstructure in this alloy essentially consists of γ and γ' phases. Figure 2 shows that, in addition to the cuboidal (or secondary) γ' with an average size of 400–500 nm, fine particles of γ' (tertiary γ') typically less than 10 nm are present within the γ channels that are less than 50–60 nm wide. The cuboidal shape of the secondary γ' particles stems from an optimal *misfit* between γ and γ'. The misfit is defined as

$$\delta = (a_{\gamma'} - a_{\gamma})/(0.5 * (a_{\gamma'} + a_{\gamma}))$$

where $a_{\gamma'}$ and a_{γ} are the cubic lattice parameters of γ' and γ, respectively. In addition to the size, morphology, and spatial distribution of γ', important microstructural issues include the composition of γ and γ' phases, and the composition gradients that may exist at γ/γ' interfaces. These issues form the focus of the study presented in this article.

Traditionally, TEM and high resolution TEM, and the associated analytical techniques of energy dispersive spectroscopy (EDS), and electron energy loss spectroscopy (EELS), have been extensively used for sub-micron scale microstructural characterization, to obtain structural, crystallographic, and analytical information. However, as the scale of interest approaches that of a few nanometers or less, it becomes difficult to overcome an inherent drawback of TEM techniques, which is the convolution of information along the beam (specimen thickness) direction. For microstructural features such as fine particles that are fully embedded within the TEM specimen thickness, there is considerable *matrix* interference making it almost impossible to obtain accurate analytical information regarding the embedded features. Whereas the lateral resolution of TEM has been continually improving and has now reached sub-Angstrom levels, the specimen thickness-induced limitations in the *depth* direction still persist. In contrast, the 3DAP is capable of single atom analytical depth resolution but relatively poor surface (lateral) resolution, and therefore has the potential to provide micro (nano) structural information that is complementary to the TEM. 3DAP microscopy is a destructive technique in which field evaporation of a needle-shaped specimen, with a tip radius typically between 20 and 50 nm, is carried out in a controlled manner leading to the production of positively charged ions from the atoms in the specimen held at a positive bias with respect to the earth and the 'position sensitive detector' (PSD). The ions are collected at the PSD which records the (x, y) positions on the detector, and the time of flight of each ion from the sample to the detector is used to identify its mass-to-charge ratio using time of flight mass spectrometry. Thus, the data acquisition process involves the collection of a series of sequential (x, y, t) data which can subsequently be reconstructed by software to give the 3-dimensional (x, y, z) positions and the mass-to-charge ratio of the ions (atoms) in the *sample*. An excellent overview of the principles and operation of different types of atom probe equipment as well as their use in nanometric scale characterization of materials can be found in several books [4, 5] and review articles [6, 7]. The role of atom probe in the study of nickel-base superalloys has been reviewed by Blavette et al. [8].

It is evident that a combination of TEM and 3DAP techniques enables a thorough investigation of materials' microstructures from the sub-micron to nanometric scales. This article outlines some of our efforts in addressing issues at these scales in DMS4 nickel-base superalloy using TEM and 3DAP.

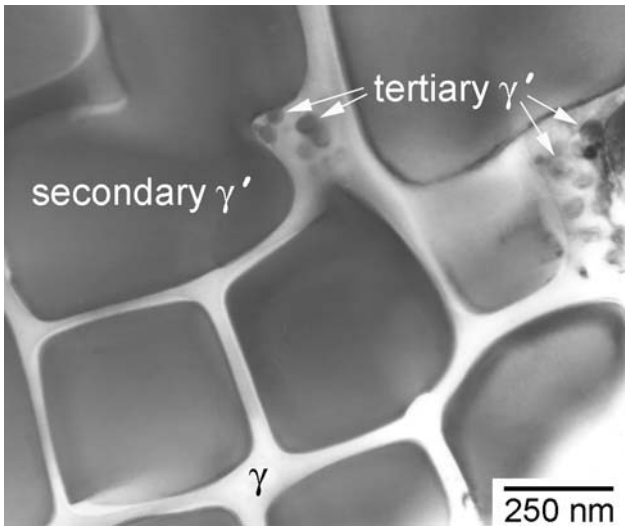

Fig. 2 TEM bright field micrograph of fully aged sample showing cuboidal secondary γ' particles, the γ channels and the presence of fine tertiary γ' particles within the channels

Experimental

The alloy was prepared by vacuum induction melting and investment cast in the form of single crystal rods using

helical crystal selector under directional solidification conditions. Samples were subjected to a complex heat treatment cycle that consisted of multi-step solutionizing (between 1,315 °C and 1,360 °C) and multi-step aging treatments (between 1,160 °C and 870 °C) [2, 3]. To obtain thin foils for TEM examination, ~200 μm thick slices were cut from sample blanks using a slow speed saw, mechanically ground to ~100 μm thickness, and subsequently twin-jet electropolished with mixed acids (by volume: 78 pct methanol, 10 pct lactic acid, 7 pct sulfuric acid, 3 pct nitric acid, and 2 pct hydrofluoric acid) electrolyte at −30 °C. The thin foils were examined in either a Philips EM430T transmission electron microscope operated at 250 kV, or a FEI Tecnai 20T transmission electron microscope operated at 200 kV. Both were equipped with EDAX energy dispersive spectroscopy systems. The atom probe specimens were prepared by a standard two-stage electropolishing procedure as described by Miller and Smith [4]. Initially, 15–20 mm long blanks with 0.3–0.5 mm diameter were cut from fully heat-treated blanks using wire EDM. In the first stage, a solution of 25% perchloric acid in glacial acetic acid was used at 5–15 V DC to thin down the shank diameter of the blanks and subsequently to obtain a rough conically shaped tip. In the second stage, the final tip was formed by pulse micropolishing, initially using a solution of 6% perchloric acid in glacial acetic acid, and subsequently using 2% perchloric acid in 2-butoxy ethanol at 5–20 V DC. Atom probe experiments were carried out employing a 3DAP with field ion microscope (FIM) instrument manufactured by Oxford nanoScience Ltd., Milton Keynes, UK (presently with Imago Scientific Instruments, Wisconsin, USA). Field ion images were recorded at a specimen temperature of 70 K with neon as the imaging gas at $\sim 2.5 \times 10^{-5}$ mbar pressure. Once a clean field ion image was obtained, the region of interest was chosen and positioned for atom probe data acquisition which was performed at pressures below 8×10^{-10} mbar at pulse repetition rates from 1 to 5 kHz using a 15% pulse fraction. Data reconstruction, analysis, and visualization were performed using the PoSAP software supplied with the instrument.

Results and discussion

Misfit determination by CBED

The cuboidal shape of the secondary γ' particles is a result of an optimal *misfit* that exists between the particles and the γ matrix. Too low a misfit leads to more spherical (non-cuboidal) particles which offer poor creep resistance while too high a misfit leads to rapid coarsening of the γ' particles thereby reducing the useful life of the component. Therefore, an optimal mismatch in lattice parameters between γ and γ', of the order of $\sim 5 \times 10^{-4}$ nm, is desirable. Therefore the determination of misfit requires techniques that are capable of measuring lattice parameters accurate to at least 0.0005 nm. Techniques that provide this level of accuracy include high-resolution X-ray diffraction (HRXRD), synchrotron diffraction and, in the TEM, a convergent beam electron diffraction (CBED) technique employing higher order Laue zone (HOLZ) lines. The CBED-HOLZ technique for determination of lattice parameters and strains is well established, for example, see [9]. The technique relies on analyzing the relative positions of the HOLZ lines, or equivalently that of HOLZ line intersections, in the transmitted disc of CBED patterns. The positions of the HOLZ lines are strongly dependent on the lattice parameters and operating conditions such as the accelerating voltage of the microscope, sample thickness, etc. Thus, for a known set of operating conditions, the lattice parameters can, at least in principle, be determined to a high level of accuracy. Although the resolution of the CBED-HOLZ technique is at least an order of magnitude poorer than that of HRXRD or synchrotron diffraction, the technique does offer the advantage of being able to provide *local* information as opposed to sample-averaged information. Thus, it becomes possible to correlate local composition to γ' morphology and the lattice misfit.

The CBED-HOLZ technique has been successfully employed in a number of investigations for determination of misfit in nickel-base superalloys [10–12] wherein it has also been established that the use of <1 1 19> orientation (~4° off <0 0 1> zone) is ideally suited. Figure 3a shows

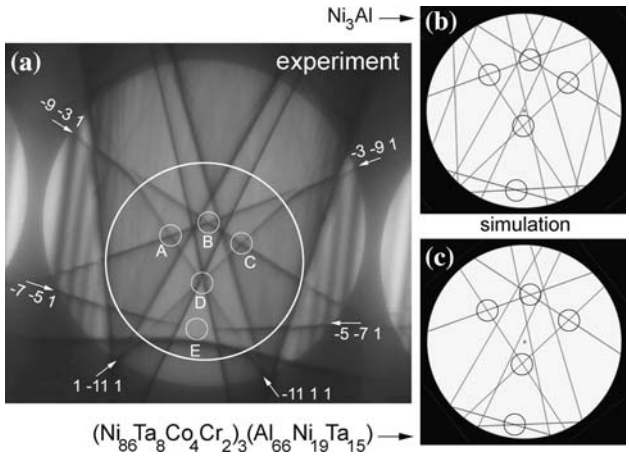

Fig. 3 CBED-HOLZ patterns near [1 1 19] orientation at 250 kV accelerating voltage: **a** experimental pattern obtained from the center of a γ' particle at −150 °C; **b** simulated pattern for pure Ni_3Al with lattice parameter $a = 0.36$ nm; and **c** simulated pattern for $(Ni_{86}Ta_8Co_4Cr_2)_3(Al_{66}Ni_{19}Ta_{15})$ with $a = 0.362$ nm. The larger circle in (**a**) marks the region shown in (**b**) and (**c**). The main HOLZ lines are indexed and HOLZ line intersections indicated with small circles labeled A–E

a CBED-HOLZ pattern obtained from the center of a typical cuboidal γ' particle in a fully aged DMS4 alloy, near [1 1 19] orientation, at a microscope-accelerating voltage of 250 kV. The experiment was done at −150 °C using a cooling holder in order to improve the sharpness of the HOLZ lines. Obviously, the lattice parameters being determined from the HOLZ experiments are specific to the temperature at which the experiment is being performed. Figure 3b shows a simulated pattern for pure Ni_3Al ($a = 0.36$ nm) in an identical orientation generated using EMS software [13]. The HOLZ lines and their intersections (A–E) are also identified in the figure. It may be noted that the intersection E is influenced by strong dynamical effects and hence was not used for the lattice parameter determination. The lattice parameter of 0.36 nm represents the closest match that was achieved for the range of lattice parameters investigated, when the composition of γ' (in the simulation) was assumed to be pure Ni_3Al. However, detailed analysis has shown that, in addition to having an indirect influence on the HOLZ patterns through an effect on the lattice parameters, the composition also appears to directly influence the HOLZ patterns (Balamuralikrishnan and Muraleedharan 2005, unpublished research). Thus, knowledge of the phase composition is essential in order to simulate patterns having a closer match to experimental results. Figure 3c shows a simulated pattern for $(Ni_{86}Ta_8Co_4Cr_2)_3(Al_{66}Ni_{19}Ta_{15})$, at the closest matching cubic lattice parameter of 0.362 nm. This composition represents, to a first approximation, the expected secondary γ' composition (including site occupancy) in DMS4, derived (Balamuralikrishnan and Muraleedharan 2005, unpublished research) from the alloy nominal composition and the partitioning behaviour of some of the alloying elements determined in an atom probe study of CMSX-4 nickel-base superalloy [14]. The simulated pattern with this composition shows a better match with experiments than that obtained from simulations of pure Ni_3Al (Fig. 3b). However, a more accurate γ' composition in the DMS4 alloy, obtained from atom probe experiments as explained in the following sections, may be used to further improve the lattice parameter accuracy. Nevertheless, the use of the CBED-HOLZ technique for γ' lattice parameter determination has been demonstrated. It should be pointed out that, due to spatial resolution considerations (extremely fine width of the γ channels as well as the presence of tertiary γ' in those channels, Fig. 2) we could not apply the technique to the γ phase. We are presently investigating possible means of overcoming these limitations.

Phase composition from TEM/EDS

Figure 4a shows EDS spectra obtained from γ' (solid) and γ (dotted) phases. Qualitatively, it can be seen that while Al and Ta partition preferentially to γ', Co, Cr, and Re partition preferentially to γ. However, there is severe peak overlap in the energy range from approximately 8 keV to 12 keV, as indicated in Fig. 4b in which all the peaks associated with the L-series of Ta, W, and Re are shown along with the K_β peak of nickel. We have found that this spectral overlap leads to large errors in the quantification of phase composition using routine quantification procedures, particularly with respect to Ta, W, and Re. The quantification accuracy may be improved either by the use of customized quantification techniques or through the use of spectra obtained from a set of standards containing known and different amounts of Ni, Ta, W, and Re. In addition to this spectral resolution limitation, obtaining spectra from γ also suffers from a spatial resolution limitation, as explained in the previous section.

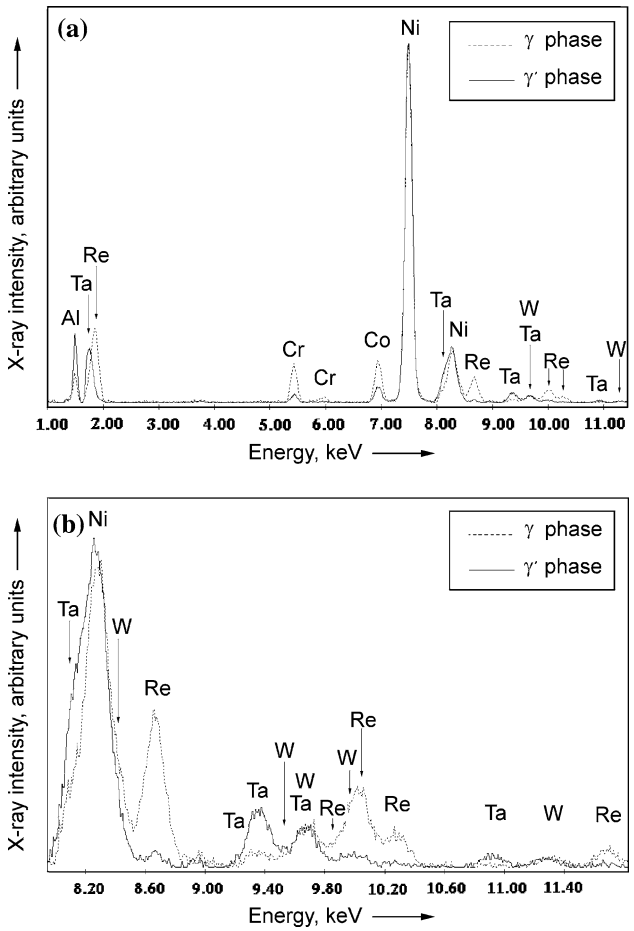

Fig. 4 EDS spectra from γ (*dotted*) and γ' (*solid*) phases illustrating the peak overlap (magnified image in inset)

Phase composition from 3DAP

The 3DAP has been effectively used to determine the alloying element partitioning between γ and γ' phases in

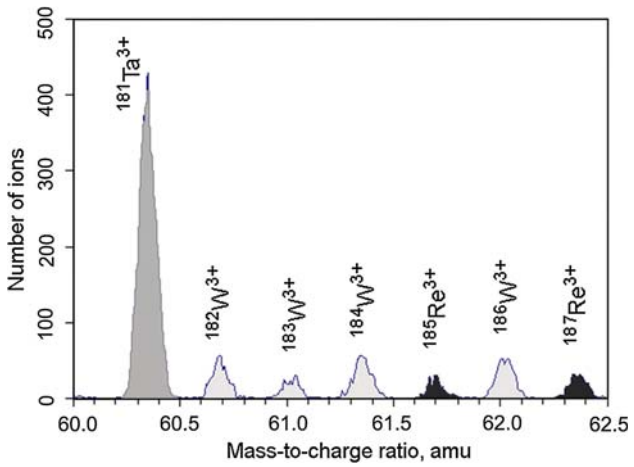

Fig. 5 Portion of mass spectrum obtained, from DMS4, using 3DAP, showing well-resolved peaks due to 3+ ions of Ta, W, and Re. The different isotopes are indicated

actual or model nickel-base superalloys [8, 14–17]. Figure 5 is a part of the mass spectrum obtained from a DMS4 sample, showing clearly resolved peaks of Ta, W,

Table 2 Composition of γ and γ' phases, and associated partition coefficients, in fully aged DMS4 alloy determined by 3DAP

	C_γ (at%)	$C_{\gamma'}$ (at%)	$K = C_\gamma/C_{\gamma'}$	$K' = C_{\gamma'}/C_\gamma$
Cr	7.10 ± 0.20	0.73 ± 0.07	9.73	0.10
Co	7.08 ± 0.20	1.35 ± 0.09	5.24	0.19
W	3.12 ± 0.14	2.32 ± 0.12	1.34	0.75
Re	8.85 ± 0.22	0.29 ± 0.04	30.52	0.03
Ta	0.59 ± 0.06	5.19 ± 0.18	0.11	9.09
Nb	2.08 ± 0.11	2.01 ± 0.11	1.03	0.97
Al	2.34 ± 0.12	16.87 ± 0.30	0.14	7.14
Ni	68.76 ± 0.37	71.11 ± 0.37	0.97	1.03

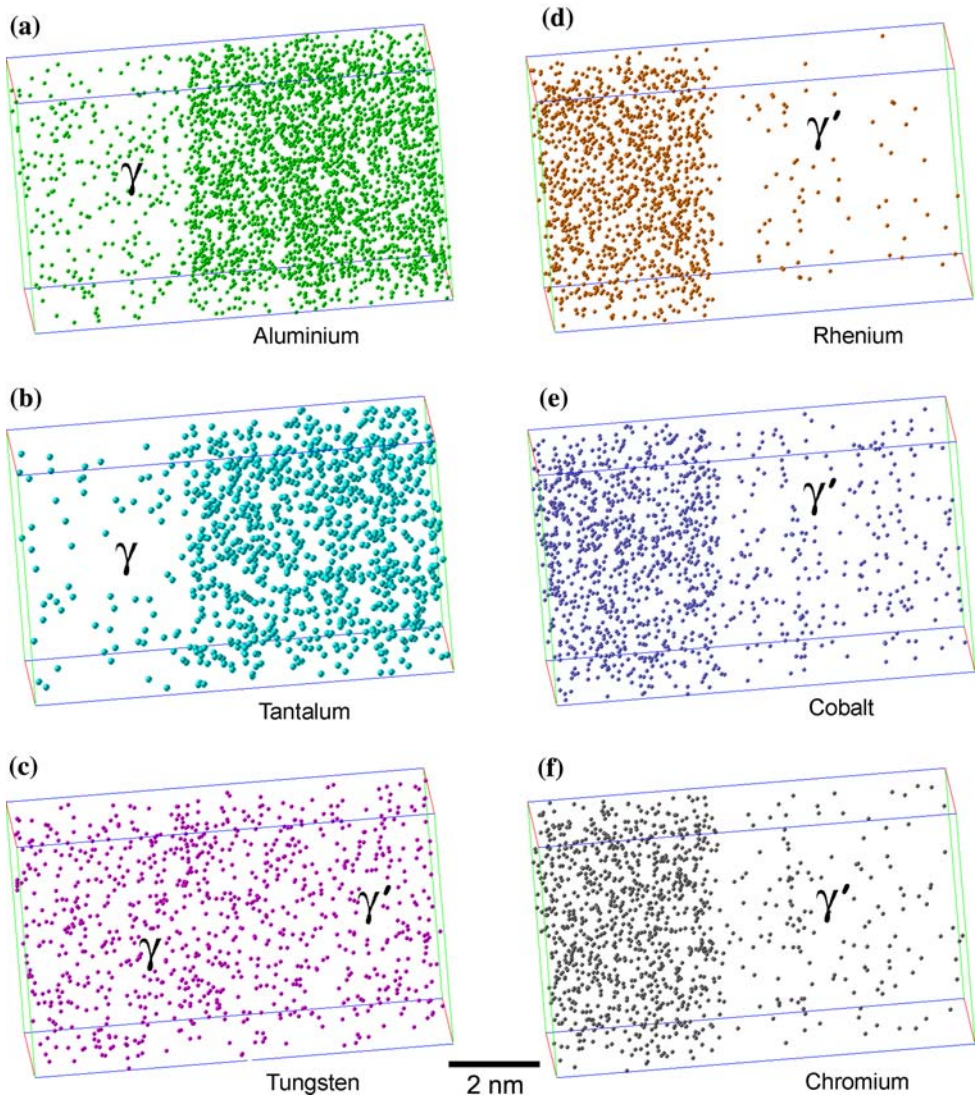

Fig. 6 Elemental atom maps in fully aged DMS4 sample showing the partitioning of the elements to γ and γ' phases: **a** Al; **b** Ta; **c** W; **d** Re; **e** Co; and **f** Cr. Ni and Nb are not shown

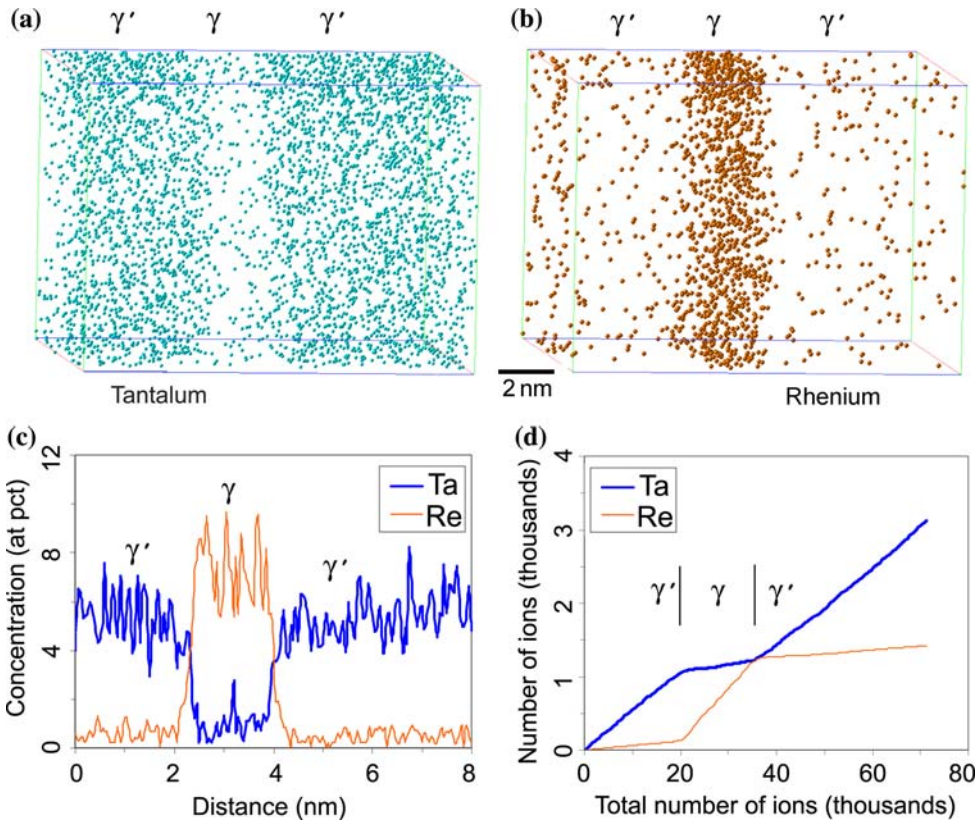

Fig. 7 Composition near γ/γ' interface in DMS4 alloy variant, in as-solutionized condition: **a**, **b** atom maps for Ta and Re, respectively; **c** composition profile; and **d** ladder diagram, for a sub-volume (see text for details) showing the presence of sharp γ/γ' interface

and Re, corresponding to the 3+ ions of the different isotopes of each species, as indicated in the figure. The peak at 60 atomic mass units, corresponding to $^{180}W^{3+}$, which has a relative abundance of only 0.13%, is almost invisible on the scale shown. Accurate determination of phase composition (and alloying element partitioning) in DMS4 is facilitated because of the absence of major overlaps of peaks in the mass spectrum for elements of interest, viz., Ni, Al, Co, Cr, Ta, W, and Re, that are present in the alloy.

Figure 6 shows the atom maps in a $10 \times 5 \times 9$ nm reconstructed *sub-volume* comprising ~30,000 ions, in a fully aged DMS4 sample. The full dataset consists of more than 500,000 ions. The known preferential partitioning behavior of Al to γ' can be used to identify γ and γ' regions (Fig. 6a). Based on this, it can be seen, qualitatively, that whereas Ta and Al preferentially partition to γ', Re, Co, and Cr preferentially partition to γ. In contrast, the distribution of W appears to show no such preference for either γ or γ'. By choosing further sub-volumes that lie entirely within either γ or γ', the compositions of the respective phases, as well as the associated partition coefficients, have been determined (Table 2). In general, the quantification confirms the visual observations on the partitioning of the different elements between γ and γ'. Ni, W, and Nb show relatively weak partitioning between γ and γ' with $K(= C_\gamma/C_{\gamma'})$ values close to 1. Further, the partitioning *trends* of all the elements are in agreement with those reported for other superalloys, for example, CMSX4 [14] and RR2100 [17]. However, the most striking feature is the strong partitioning of Re[1] to γ, with $K \sim 30$. In contrast, K values between 10 and 20 have been reported for most second and third generation superalloys in their standard heat-treated condition. Both CMSX4 (containing 3 wt% Re) and RR2100 (containing 6.4 wt% Re), which are representative of second and third generation superalloys, have K values of 16–17 [14, 17]. It must be emphasized that the present results are only indicative and should not be considered as conclusive, as only few samples of DMS4 have been analyzed to date. Nevertheless, the K values for Re, in all the cases are found to range between 25 and 30 which appears to be quite high. Further study is in progress to confirm the observed results.

Compositions and composition gradients at γ/γ' interfaces

Figure 7 shows the atom maps for Ta (Fig. 7a) and Re (Fig. 7b) in an as-solutionized sample. The alloy is a DMS4 variant in which the Co content has been increased to 8 wt%, mainly at the expense of Ni. The atom maps reveal the presence of a γ channel bound on either side by γ' phase. The composition profile (Fig. 7c) shows that the

[1] The partitioning of rhenium is of considerable interest, as rhenium is known to strongly influence the mechanical properties [1].

interface between γ and γ' is rather sharp. This profile is for a sub-volume of 8 nm length commencing at 2 nm from the left in Fig. 7a and b. The concentration of Re jumps abruptly from about 1 at% in γ to nearly 8 at% in γ' within a fraction of a nanometer. The corresponding change in Ta is less abrupt, but still happens within 2–3 atomic layers. This can also be seen from the *ladder diagram* (Fig. 7d, for the same region as in Fig. 7c) in which the cumulative number of ions of Ta and Re are plotted against the cumulative total number of ions collected. The slopes in the γ and γ' regions directly yield the atomic concentration of the element. It is seen from this figure also that the γ/γ' interface is sharp as indicated by the sudden change of slope at the interface. The concentration in γ' tends to become uniform after a few atomic layers from the interface. This has been quantitatively confirmed by sub-volume composition analysis of γ' as a function of distance from the interface (Balamuralikrishnan and Muraleedharan 2007, unpublished research).

Summary

Several microstructural factors spanning multiple length scales, from the order of a few tens of micrometers to fractions of a nanometer, influence the properties and therefore the performance in service of nickel-base superalloys. In this study, we have illustrated how the TEM and 3DAP techniques might be utilized to address issues at submicron and nanometric scales in a specific nickel-base superalloy, namely, DMS4. We have been able to, for the first time, determine the compositions of γ and γ' phases and thereby the alloying element partitioning in DMS4. These results suggest an unusually strong partitioning of Re to γ. Further, all observed γ/γ' interfaces have been found to be sharp, with the Re concentration changing abruptly at the γ/γ' interface. It must however be noted that the results presented here are to be considered as illustrative, and not conclusive. More experiments, particularly, those pertaining to composition determination using 3DAP, are required for statistical validation and confirmation of the current observations. In addition, characterization of samples as a function of heat treatment would be required to obtain a comprehensive understanding of the microstructural changes during processing.

Acknowledgements This research was funded by Defence Research and Development Organization (DRDO), India, under Project DMR-254, 'Science and Design of Materials at Atomic Scale'. The permission of Director, Defence Metallurgical Research Laboratory (DMRL), Hyderabad, to publish the results is gratefully acknowledged. We acknowledge the contributions of Mr L. Srivardhan (for heat treatment) and Mr Mohan P. Pathak (for 3DAP experiments). The authors are grateful to Professor S. Ranganathan, Indian Institute of Science, and Dr. D. Banerjee, Chief Controller, DRDO for their keen interest and constant encouragement.

References

1. Reed RC (2006) The superalloys—fundamentals and applications. Cambridge University Press, Cambridge
2. Das N (1999) US Patent 5916384
3. Das N, Singh S, Hazari N, Chaterjee D, Praveen VVNSSC (2007) Met Mater Process 19:189
4. Miller MK, Smith GDW (1989) Atom probe microanalysis: principles and applications to materials problems. Materials Research Society, Pittsburgh
5. Miller MK (2000) Atom probe tomography: analysis at the atomic level. Kluwer/Plenum, New York
6. Hono K (2002) Prog Mater Sci 47:621
7. Seidman D (2007) Annu Rev Mater Res 37:127
8. Blavette D, Cadel E, Deconihout B (2000) Mater Charact 44:133
9. Spence JCH, Zuo JM (1992) Electron microdiffraction. Plenum Press, New York
10. Voelkl R, Glatzel U, Feller-Kniepmeier M (1998) Acta Mater 46:439511
11. Schulze C, Feller-Kniepmeier M (2000) Mater Sci Eng A 281:204
12. Schulze C, Feller-Kniepmeier M (2001) Scripta Mater 44:731
13. Stadelmann P (2001) Java electron microscopy software (JEMS) Version 1.0724W2001
14. Wanderka N, Glatzel U (1995) Mater Sci Eng A 203:69
15. Warren PJ, Cerezo A, Smith GDW (1998) Mater Sci Eng A 250:88
16. Rusing J, Wanderka N, Czubayko U, Naundorf V, Mukherji D, Rosler J (2002) Scripta Mater 46:235
17. Reed RC, Yeh AC, Tin S, Babu SS, Miller MK (2004) Scripta Mater 51:327